$FeGe_{1-x}Sb_x$: A series of kagome metals with noncollinear antiferromagnetism

Jiale Huang,[1,2] Chenglin Shang,[1,2] Jianfei Qin,[3] Feihao Pan,[1,2] Bingxian Shi,[1,2] Jinchen Wang,[1,2] Juanjuan Liu,[1,2] Daye Xu,[1,2] Hongxia Zhang,[1,2] Hongliang Wang,[3] Lijie Hao,[3] Wei Bao,[4] and Peng Cheng[1,2,*]

[1]*Laboratory for Neutron Scattering and Beijing Key Laboratory of Optoelectronic Functional Materials and MicroNano Devices, Department of Physics, Renmin University of China, Beijing 100872, China*

[2]*Key Laboratory of Quantum State Construction and Manipulation (Ministry of Education), Renmin University of China, Beijing 100872, China*

[3]*China Institute of Atomic Energy, P.O. Box 275-30, Beijing 102413, China*

[4]*Department of Physics, City University of Hong Kong, Kowloon, Hong Kong 999077, China*

(Received 21 September 2023; revised 26 October 2023; accepted 16 November 2023; published 28 November 2023)

Kagome metals are important for exploring emergent phenomena due to the interplay between band topology and electron correlation. Motivated by the recent discovery of charge density waves in the kagome lattice antiferromagnet FeGe, we investigate the impact of Sb doping on the structural, charge, and magnetic order of FeGe. The superlattice distortion induced by charge order disappears with only slight Sb doping (∼1.5%) down to 80 K. The antiferromagnetic ordering temperature gradually shifts to 280 K for $FeGe_{0.7}Sb_{0.3}$. For $FeGe_{1-x}Sb_x$ with $x \geqslant 0.1$, crystal structures with a slightly distorted Fe kagome lattice are formed. A significant change in magnetic anisotropy from easy axis to easy plane with increasing x is identified from magnetization measurements. Interestingly, neutron diffraction reveals noncollinear antiferromagnetic structures widely exist below T_N for all samples with $x \geqslant 0.1$. These noncollinear magnetic orders could possibly be unconventional and result from on-site repulsion and filling conditions of the kagome flat band, as predicted by a recent theoretical work.

DOI: 10.1103/PhysRevB.108.184431

I. INTRODUCTION

The kagome lattice hosts a peculiar electronic structure with the coexistence of Dirac cones, flat bands, and van Hove singularities [1–3]. In metallic materials with 3*d* transitional metal kagome networks, various novel emergent phenomena, including superconductivity, magnetism, the anomalous Hall effect, and charge order, have been observed in recent years [4–12]. Therefore, they have become an important platform to explore correlated quantum states intertwined with topological band structures.

The kagome charge density wave (CDW) has drawn great attention due to its many-body correlations and topological features [1]. It was initially discovered in kagome superconductors AV_3Sb_5 ($A = $ K, Cs, Rb) and found to break time-reversal symmetry with the absence of any long-range magnetic order [13]. This CDW order is considered to be unconventional, arising from Fermi surface nesting of van Hove singularities and hosting a chiral flux phase which induces the anomalous Hall effect [14–18]. On the other hand, the magnetism in kagome metals may also be unconventional. It has been proposed that the large density of states from the kagome flat bands could induce ferromagnetism [6,7]. However, the coexistence and interplay between CDW and long-range magnetic order was not observed in kagome metals until recently. Hexagonal FeGe with a kagome lattice was reported to display a CDW transition at 100 K coupled to the long-range antiferromagnetic order below $T_N = 410$ K [19].

Spectroscopic experiments have revealed an intimate interaction between the CDW order and magnetism in FeGe [20,21]. However, the origin of this CDW order remains elusive, along with its relation to the anomalous Hall effect and magnetic order. Furthermore, a recent Hartree-Fock analysis showed that unconventional noncollinear antiferromagnetic (AFM) order may exist in the magnetic phase diagram of FeGe tuned by on-site repulsion and flat-band filling [22]. For materials with noncollinear antiferromagnetism, the scalar spin chirality or a nonzero Berry curvature with spin-orbital coupling may induce a strong anisotropic anomalous Hall effect and spin Hall effect [23,24]. These intriguing effects have been realized in Mn_3Sn and Mn_3Ge with the kagome lattice and have received great research interest [10,25,26]. Although a large number of magnetic kagome metals have already been discovered, noncollinear antiferromagnets seem to be quite rare besides the Mn_3X ($X = $ Ge, Sn, Ga, Ir) material family [24,27,28].

Here we report the Sb doping effect on FeGe and map the phase diagram of $FeGe_{1-x}Sb_x$ ($0 < x < 0.4$). Using x-ray, transport, magnetic susceptibility, and neutron scattering measurements, we characterize the evolution of the crystal structure, CDW, and magnetic order with Sb doping. Intriguingly, noncollinear AFM structures are found to widely exist in $FeGe_{1-x}Sb_x$. Studies on this new series of kagome metals not only may provide opportunities to understand the origin of the unconventional CDW and its interplay with magnetic

*Corresponding author: pcheng@ruc.edu.cn

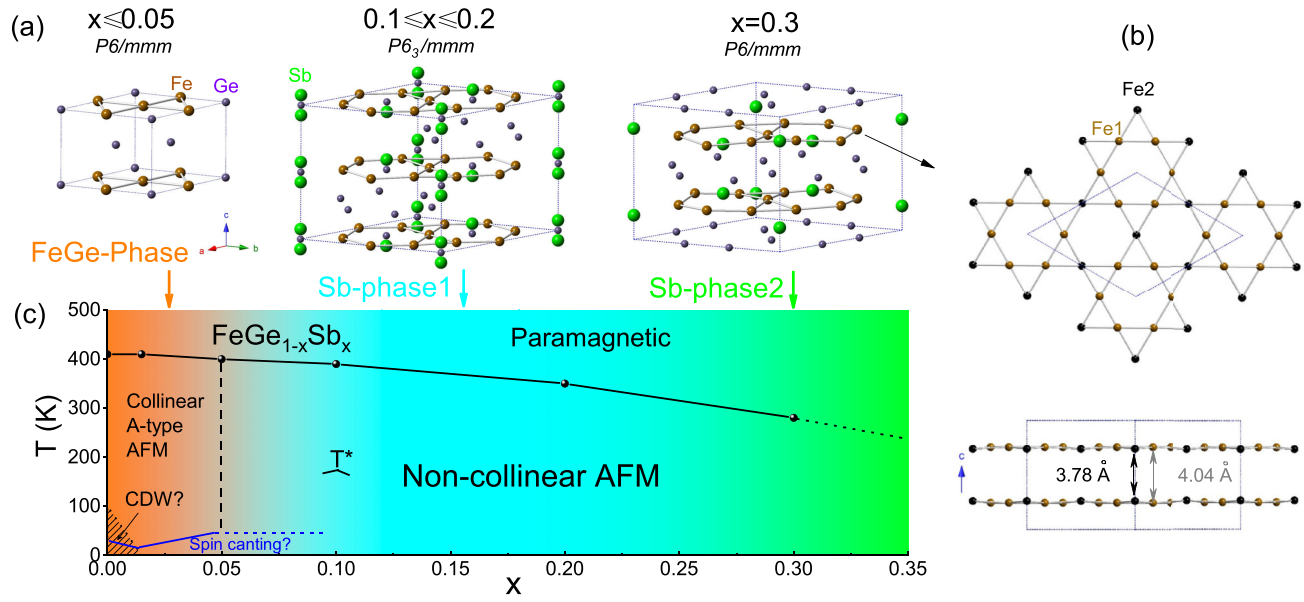

FIG. 1. (a) Illustration of the crystal structures of $FeGe_{1-x}Sb_x$ at different doping concentrations x. The crystal unit cell is marked by blue dotted lines. For $x > 0.1$, some adjacent atoms in extended cells along the c axis are also shown for clarity. (b) For $x = 0.3$, the Fe kagome lattice in the ab plane is shown on the top. On the bottom, another view shows that the kagome lattice is slightly distorted along the c axis. (c) Composition-temperature phase diagram for $FeGe_{1-x}Sb_x$.

order in FeGe but also could stimulate future research on exploring novel topological and correlated phenomena driven by kagome physics.

II. METHODS

Polycrystalline $FeGe_{1-x}Sb_x$ samples were synthesized by solid-state reaction of stoichiometric Fe, Ge, and Sb powders at 700 °C for 4 days, then furnace cooled to room temperature. The samples are characterized by powder x-ray diffraction (XRD) using a Bruker D8 Advance x-ray diffractometer. Rietveld refinement showed that the samples with $x < 0.2$ appeared to be phase pure, and some minor impurity phases, including Fe_3Ge_2 and Sb, could be identified for samples with higher x [29].

Single crystals of $FeGe_{1-x}Sb_x$ were grown by the chemical vapor transport method using synthesized polycrystalline samples similar to those in previous reports [19]. The obtained crystals are three-dimensional, with a typical size of 1 mm. Most crystals are rod shaped with a 1 or 2 mm size along the c axis, while the ab plane has a very small size (0.3×0.3 mm^2). For $x = 0.3$, we accidentally grew a crystal with a very large ab plane (1×2 mm^2). The elemental composition of all single crystals were characterized with energy dispersive x-ray spectroscopy (EDS; Oxford X-Max 50). The doping concentration x determined by EDS may have a slight deviation from the nominal doping value. For example, single crystals with nominal $x = 0.01$ are determined to be $x = 0.015$ by EDS. All values of x refer to the EDS values in this paper, except for polycrystalline samples. The crystal structures of single crystals were all examined by a Bruker D8 VENTURE single-crystal diffractometer using Cu $K\alpha$ radiation in a fast scan mode; the crystal symmetry and lattice parameters were determined by refinement using APEX3. The low-temperature (80 K) single x-ray diffraction was performed on an $x = 0.015$ crystal using a Rigaku XtaLAB-Synergy-R spectrometer to check the possible CDW superlattice peak.

Magnetization and electrical transport measurements were carried out on a Quantum Design MPMS3 and PPMS-14T, respectively. Powder neutron diffraction experiments were carried out on the Xingzhi cold neutron triple-axis spectrometer at the China Advanced Research Reactor (CARR) [30]. About 4–6 g of $FeGe_{1-x}Sb_x$ powder for each doping were used in the neutron experiments. The incident neutron energy was fixed at 16 meV. The program FULLPROF SUITE was used in the representational analysis and Rietveld refinement of neutron powder diffraction data [31].

III. RESULTS AND DISCUSSION

There are three polymorphs for FeGe with monoclinic, hexagonal, and cubic structures. Cubic FeGe is well known as a magnetic skyrmion crystal [32]. Hexagonal FeGe is the only polymorph with a kagome lattice, and we refer to it as the FeGe phase in this paper. It adopts a CoSn-type crystal structure with alternating stacking of the Fe_3Ge kagome layer and the Ge honeycomb layer. Our XRD analysis of both single crystals and polycrystalline samples reveals that $FeGe_{1-x}Sb_x$ maintains the crystal structure of FeGe for $x \leqslant 0.05$. However, at a higher doping level, the results show that Sb does not simply replace Ge and new chemical phases are formed, as illustrated in Fig. 1(a). The details of structural refinement results are given in the Supplemental Material [29]. It should be mentioned that the crystal structures of $FeGe_{1-x}Sb_x$ with $x \geqslant 0.1$ were initially determined by Mills and Mar in an early publication [33], and their results are consistent with our results here. We call $FeGe_{1-x}Sb_x$ with $0.1 \leqslant x \leqslant 0.2$ Sb phase 1 and that with $x = 0.3$ and 0.33 Sb phase 2. As shown in Fig. 1(a), the unit cells of new phases are all about six times larger than that of the FeGe phase ($a' = \sqrt{3}a$, $c' = 2c$). Sb

TABLE I. Room temperature lattice parameters for $FeGe_{1-x}Sb_x$ obtained from single-crystal XRD.

Sample type	x	a (Å)	c (Å)
Single crystal	0	5.003(5)	4.055(3)
Single crystal	0.015	5.031(70)	4.055(7)
Single crystal	0.05	5.063(8)	4.056(11)
Single crystal	0.1	8.830(4)	8.108(2)
Single crystal	0.2	8.930(39)	7.990(46)
Single crystal	0.3	8.976(5)	7.952(6)

phase 1 adopts a different space group, $P6_3/mmm$. The Ge atoms in the honeycomb layer are gradually removed, while the Sb atoms form Sb_2 pairs whose center of mass lies at the center of hexagons in the Fe_3Ge kagome plane. The occupancy of Sb_2 pairs is only partial. For Sb phase 2, the structure can be best described using the chemical formula Fe_3Ge_2Sb. Compared with the FeGe phase, the Ge honeycomb layer in Sb phase 2 remains unchanged, while the Ge atoms in the Fe_3Ge kagome layer are completely replaced by Sb atoms whose positions have an ordered shift along the c axis.

Next, we focus on the structural details in the Fe kagome lattice. As shown in Fig. 1(b), different from the FeGe phase, the Fe ions occupy two inequivalent Wyckoff positions for both Sb phase 1 and Sb phase 2. The nearest Fe1-Fe1 distance between two adjacent kagome layers is larger than the Fe2-Fe2 distance, as illustrated in Fig. 1(b). This results in slight distortion of the kagome layer along the c axis compared with the perfectly flat kagome net in the FeGe phase.

Figure 1(c) presents the phase diagram of $FeGe_{1-x}Sb_x$, which shows the evolution of different solid phases with doping concentration. The room temperature lattice parameters determined from XRD for different samples are presented in Table I. A general tendency is that with increasing x, the a-axis lattice constant increases while the c-axis constant decreases. The lattice constants of the FeGe phase can be transformed by using the formulas $a' = \sqrt{3}a$ and $c' = 2c$ for comparison. It seems that the doping of Sb causes a lattice compression effect along the c axis. As a result, the nearest Fe-Fe distance in one kagome layer increases from 2.54 Å for FeGe to 2.60 Å for Fe_3Ge_2Sb. The buckled kagome structure of Fe_3Ge_2Sb was also confirmed by a very recent publication [34]. For the physical properties of $FeGe_{1-x}Sb_x$, as far as we know, only that of Fe_3Ge_2Sb (close to our samples with $x = 0.3$ and 0.33) was reported recently [34].

FeGe serves as a very rare example for the coexistence of CDW and AFM order. We first investigate how these orders would evolve with Sb doping via magnetization measurements. Figures 2(a) and 2(b) show the temperature-dependent magnetic susceptibility of single crystals with the FeGe phase. Consistent with a previous report, for the parent compound FeGe, there is a hump at 100 K in the $\chi(T)$ curve under $H \parallel ab$ due to the development of CDW order at this temperature [19]. However this feature disappears with $x = 0.015$, indicating suppression of the CDW with Sb doping. More evidence for the suppression of the CDW comes from the single-crystal diffraction data at $T = 80$ K (inset in Fig. 3); the absence of any superlattice peaks at $Q_{CDW} = (H + 0.5, 0, L + 0.5)$ suggests the charge order disappears at

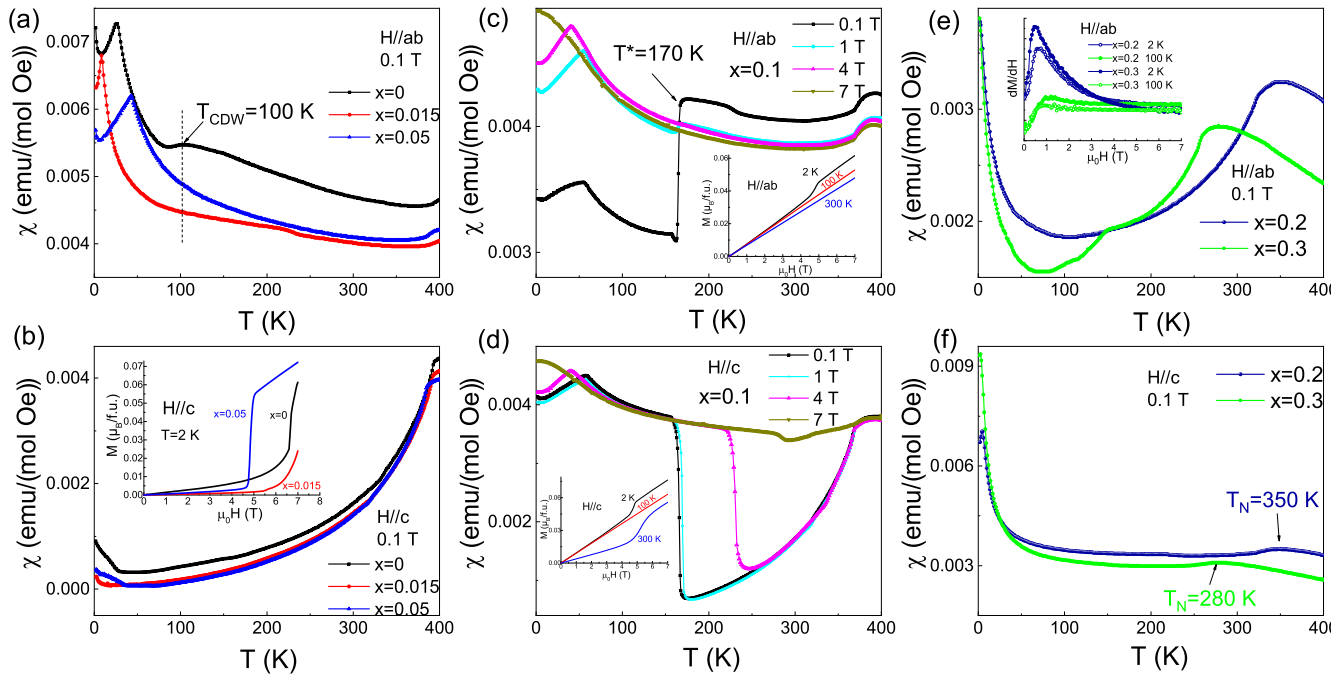

FIG. 2. Temperature-dependent magnetic susceptibilities for $FeGe_{1-x}Sb_x$ single crystals under magnetic field applied parallel to the ab plane and along the c axis in the zero-field-cooling mode. The data for $x = 0$, 0.015, and 0.05 with the FeGe phase are plotted in (a) and (b). For $x = 0.1$ with Sb phase 1, the anomaly at $T^* = 170$ K and its evolution with field can be seen in (c) and (d). The data of $x = 0.2$ and 0.3 are shown in (e) and (f). The insets show the isothermal $M(H)$ curves measured at different fields, and dM/dH as a function of field is plot in the inset of (e) for a clear view of field-induced magnetic transition.

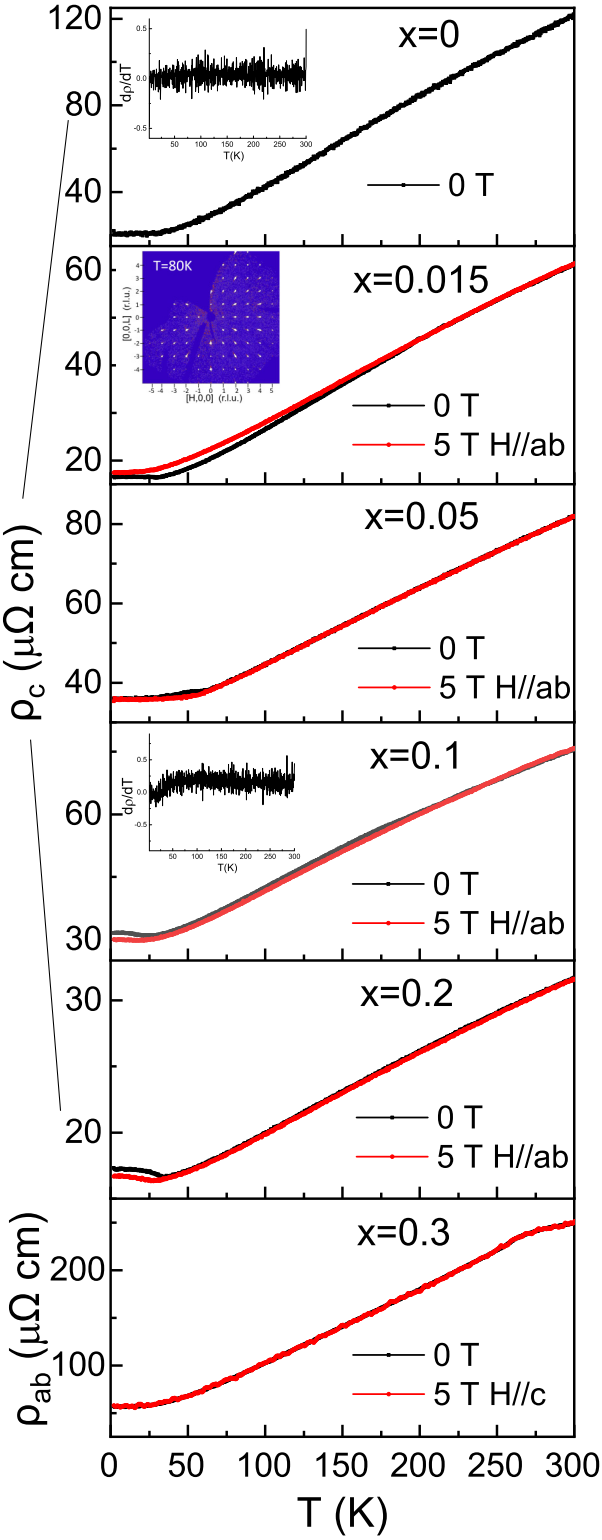

FIG. 3. Temperature-dependent resistivity of $FeGe_{1-x}Sb_x$ single crystals under $\mu_0 H = 0$ and 5 T. The insets show the $d\rho/dT$ curves for $x = 0$ and $x = 0.1$, as well as the precession image in the $H0L$ plane for $x = 0.015$ at 80 K from single-crystal x-ray diffraction.

least above 80 K. This result shows that slight Sb doping will have a strong impact on the charge order of FeGe. In contrast, for other kagome metals such as CsV_3Sb_5, CDW clearly exists above 80 K with various chemical dopings up to 3% [35,36].

In addition, FeGe was reported to have a spin-flop transition under $H \parallel c$. It is found that the transition field shifts from 7 to about 5 T at 2 K, as shown in the inset in Fig. 2(b).

As revealed by Fig. 2, the AFM transition temperature is gradually suppressed to lower temperature with increasing x. T_N is determined to be 350 K for $x = 0.2$ and 280 K for $x = 0.3$. Another important feature is that, for samples with the FeGe phase, the susceptibility has a much sharper drop below T_N under $H \parallel c$, in contrast to that under $H \parallel ab$. This is a typical feature for antiferromagnets with ordered moments aligned along the c axis. However, for samples with Sb phase 1 and Sb phase 2, this feature is reversed. The susceptibility drop is much sharper under $H \parallel ab$ for $x = 0.2$ and 0.3 [Figs. 2(e) and 2(d)], which suggests the magnetic moments tend to lie in the ab plane. This doping-induced change in the magnetic anisotropy is also confirmed by the following neutron diffraction studies. In addition, a sudden jump in susceptibility occurs at $T^* = 170$ K under $\mu_0 H = 0.1$ T. This susceptibility anomaly has a quite interesting field-dependent behavior, as it moves to higher temperature with increasing field along $H \parallel c$ but becomes invisible under higher field along $H \parallel ab$. It is likely a temperature-driven spin-reorientation transition or is caused by two magnetic phases with different magnetic anisotropies, as the $x = 0.1$ sample lies on the border between easy-axis and easy-plane magnetic anisotropy. In addition, magnetic field induced spin-flop transitions could be identified for $x = 0.1$ under $H \parallel ab$ and $H \parallel c$ from the $M(H)$ curves in the insets in Figs. 2(c) and 2(d). For $x = 0.2$ and 0.3, field-induced spin-flop transitions may exist under $H \parallel ab$, as revealed by the dM/dH curves in the inset in Fig. 2(e), whereas similar features are not observed in the $M(H)$ curves for $H \parallel c$ within the field limit.

Next, several additional features in the $\chi(T)$ curves should be discussed. For FeGe, there is a cusp at 26 K in the $\chi_{ab}(T)$ curve due to the emergence of a double-cone spin canting phase according to previous investigations [19,37]. This cusp shifts to 9 K for $x = 0.015$ and then to 43 K for $x = 0.05$, which may represent the change in the temperature of the spin canting phase with doping. There is also a cusp at around 50 K for $x = 0.1$; however, the following neutron diffraction data show that the previously reported double-cone canting phase no longer exists below 50 K. Additionally, for $x = 0.015$, there is a weak kink at around 220 K. It is found that this kink becomes much weaker after we polish the crystal surface. Therefore, it should come from some impurity like $FeGe_2$, which has a magnetic transition at a similar temperature [38]. The weak kink for $x = 0.1$ at 220 K under 0.1 T in Fig. 2(c) should also result from the same impurity. There is another kink at 150 K for $x = 0.3$ under $H \parallel ab$, which is probably caused by some unknown impurity as it disappears in a smaller crystal under the same measuring conditions.

Temperature-dependent electrical resistivities are displayed in Fig. 3. Due to the rodlike crystal dimension described in the last section, for $0 \leqslant x \leqslant 0.2$, we can make the electric contacts only along the c axis and measure ρ_c. For a crystal with $x = 0.3$, the large size of the ab plane allows us to measure ρ_{ab}. For FeGe with the charge order, a kink occurs at the CDW transition temperature in the $d\rho_{ab}/dT$ curve, as reported previously [19]. However, this feature disappears in

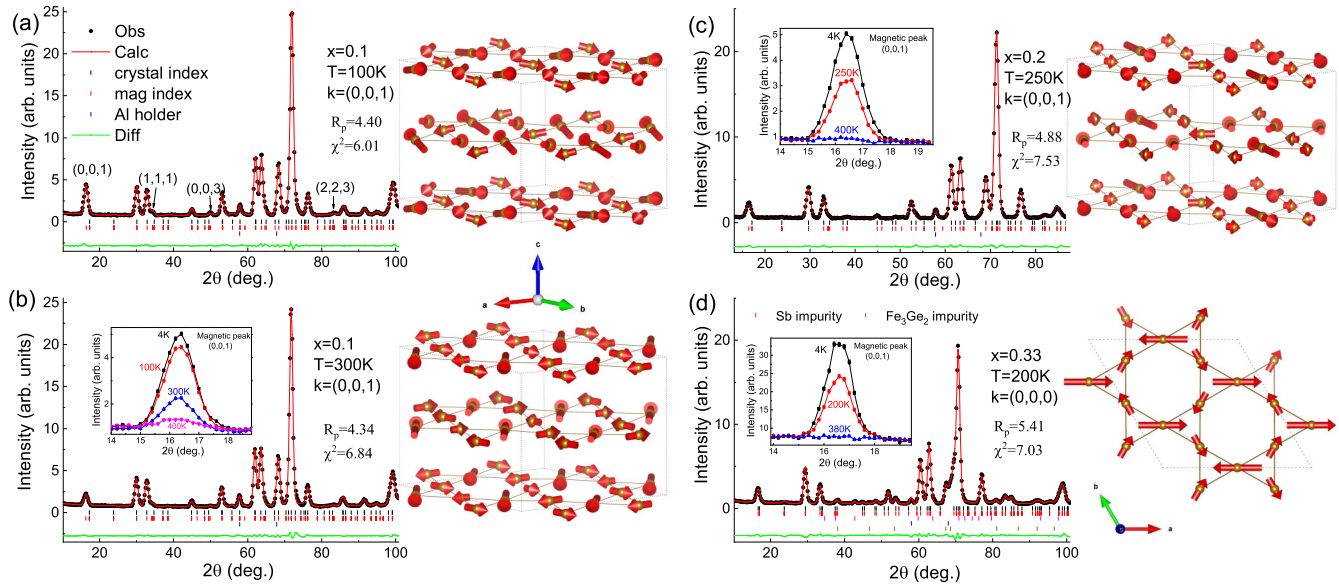

FIG. 4. Neutron diffraction patterns, Rietveld refinement results, and corresponding magnetic structures for $x = 0.1$, 0.2, and 0.33 at different temperatures. The indices of four magnetic Bragg peaks are labeled in (a). The insets in (b), (c), and (d) show the (0,0,1) magnetic peak at different temperatures. The magnetic unit cell is marked by dotted lines, and solid lines indicate the nearest Fe-Fe bond in the *ab* plane.

the $d\rho_c/dT$ curves for both $x = 0$ and $x = 0.015$ (inset in Fig. 3). So it is not possible to use this feature to verify the existence of the CDW transition.

For $x = 0.1$, no distinguishable anomaly is identified in the $d\rho_c/dT$ curve across the susceptibility anomaly at $T^* = 170$ K. A weak negative magnetoresistance (MR) could be observed below T^* and becomes notable below 30 K. Interestingly, the MR is positive for $x = 0.015$ and nearly zero for $x = 0.3$; negative MR becomes visible only for $x = 0.1$ and 0.2. We speculate that the MR behavior might be associated with the magnetic structure; magnetic field may reduce the strong spin scattering caused by the noncollinear AFM structure and result in negative MR. In addition, for both $x = 0.1$ and 0.2, an upturn of resistivity occurs below 30 K, which may possibly be due to the disorder-induced localization effect as these samples with Sb phase 1 have significant atomic vacancies in the Ge and Sb sites. For $x = 0.3$, a kink is observed at around 270 K, indicating the impact of the AFM transition on the transport property.

Next, we present powder neutron diffraction results for $x = 0.1$, 0.2, and 0.33. For all three samples, the most prominent and well-defined magnetic Bragg peak is indexed as (0,0,1), as seen from the insets in Fig. 4. According to the basic magnetic neutron scattering rules, if the ordered moments strictly lie parallel to the c axis, then (0,0,1) should have no intensity contribution from magnetic scattering, which is the case for FeGe between 400 and 60 K, as seen from previous neutron scattering experiments [19,37,39]. Note that since the c-lattice constant is doubled for $FeGe_{1-x}Sb_x$ compared with that of FeGe, (0,0,1) for $x \geqslant 0.1$ should be considered to be (0,0,0.5) for FeGe. So the significant magnetic contribution for (0,0,1) clearly means that the ordered moments of $FeGe_{1-x}Sb_x$ should have dominant in-plane components.

For $x = 0.1$ and 0.2 with Sb phase 1, (0,0,1) and other notable magnetic peaks, including (1,1,1), (0,0,3), and (2,2,3), should be in structural extinction [Fig. 4(a)]. This set of magnetic peaks is well defined by a propagation vector $\mathbf{k} = (0, 0, 1)$. We employed the BASIREPS program to carry out the representational analysis [31]. The result reveals 12 irreducible representations (IRs) for Fe1 and 6 IRs for Fe2 which are compatible with this propagation vector. Each IR describes a possible magnetic model, and we find that only one IR for both Fe1 and Fe2 could give the best fit of the diffraction data; the fitting with other IRs yields unacceptable R_P and χ^2 factors. This IR is two-dimensional with six basic vectors. The refinement results and corresponding magnetic structure for $x = 0.1$ (100 and 300 K) and $x = 0.2$ (250 K) are shown in Figs. 4(a)–4(c). Apparently, all magnetic structures are noncollinear, and the ordered moments at different Fe sites range from $\sim 1\mu_B$ to $\sim 4\mu_B$. For $x = 0.1$ at 100 K, the ordered moments have small components along the c axis (less than $0.9\mu_B$), which makes the AFM structure noncoplanar. However, at 300 K, the c-axis component becomes negligibly small (less than $0.01\mu_B$), and the orientation of the in-plane components also has some changes. For $x = 0.2$ at 250 K, the c-axis component is zero, and the AFM structure is coplanar. This result is consistent with the change in magnetic anisotropy from easy axis to easy plane with increasing x observed in the susceptibility data. It also should be mentioned that the magnetization data for $x = 0.1$ indicate the ordered moment should have a much larger c-axis component than that determined from neutron diffraction at 300 K. This inconsistency may possibly be due to some kind of phase separation or the limited resolution of powder neutron data.

The AFM structures at 4 K (see Fig. S3 in the Supplemental Material) are similar to that at high temperatures since the magnetic peaks are the same, with only some intensity enhancement. Specifically, at different temperatures, the basic vectors used to fit the neutron data are the same. Their coefficients will have some difference due to the intensity

change in the magnetic Bragg peaks; therefore, the moment size and direction of the corresponding magnetic structure derived from the linear combination of the basic vectors may have certain changes. This might explain the susceptibility anomaly at 170 K and cusp at 50 K for $x = 0.1$. Detailed data for the magnetic structures of all samples at different temperatures derived from refinement are recorded as MCIF files provided in the Supplemental Material.

For $x = 0.33$ with Sb phase 2, the indexed magnetic peaks are similar, but they are no longer in structural extinction due to the different crystal symmetry, so the propagation vector $\mathbf{k} = (0, 0, 0)$ is chosen. A similar representation analysis and refinement process also reveal that only one IR (two dimensions with six basic vectors) could best fit the diffraction data. Interestingly, for all the AFM structures in Sb phase 1, the in-plane components of the ordered moments are antiparallel between adjacent layers, suggesting an interlayer AFM interaction. However, for $x = 0.33$, the in-plane basic vectors of the only IR which could fit the data are parallel to each other for atoms with the same z-axis coordinate, which yields a magnetic structure with interlayer ferromagnetic coupling. The spin configurations at 200 and 4 K are illustrated from a view in the *ab* plane in Figs. 4(d) and S3, respectively, with only a slight moment size difference. The spins are coplanar and aligned in a 120° AFM-type triangle.

We should mention that, typically, for a complex noncollinear AFM structure, neutron diffraction on single crystals might be essential for accurate determination of the magnetic structures. Currently, the limited size of $FeGe_{1-x}Sb_x$ is hindering us from moving forward. Although the results of powder neutron diffraction may have certain fitting errors, our results could at least confirm the existence of a noncollinear magnetic structure. Actually, all the basic vectors of the possible IRs have noncollinear components in the *ab* plane; therefore, a noncollinear AFM structure is inevitable for the propagation vector determined by the indices of magnetic peaks.

Finally, we would like to discuss two aspects of the above results. First of all, since slight Sb doping could have a strong impact on the CDW order, it may provide new opportunities to uncover the origin of the CDW in FeGe. A recent angle-resolved photoemission spectroscopy (ARPES) study on FeGe proposed that magnetism-induced band-splitting pushes the van Hove singularities to the Fermi level, resulting in the formation of an unconventional charge order [20]. So it would be important to study how the band structure would be affected by slight Sb doping via ARPES and band calculations, which may provide critical information about the origin of the CDW order.

Second, a recent theoretical work predicted that an evolution from intralayer ferromagnetism to 120° AFM and noncoplanar spin orders could be realized in kagome metals by tuning on-site repulsion and flat band fillings [22]. FeGe was proposed in the border of these noncollinear AFM orders, as shown in the theoretical phase diagram [22]. These intriguing unconventional noncollinear AFM orders that are closely related to the kagome flat band might be realized in $FeGe_{1-x}Sb_x$, as demonstrated by our results, although additional theoretical and experimental evidence is needed for final confirmation. For kagome insulators, the noncollinear AFM structures are closely related to the frustration of magnetic interactions; whether frustration may be involved in the itinerant system $FeGe_{1-x}Sb_x$ should also be considered in future theoretical works. Noncollinear AFM structures are very rare in kagome metals besides the Mn_3X material family [24,27,28]. Our results may stimulate future research on exploring anomalous Hall and spin Hall effects in $FeGe_{1-x}Sb_x$, which may be induced by noncollinear antiferromagnetism.

IV. CONCLUSIONS

In summary, the physical properties and phase diagram of the kagome metals $FeGe_{1-x}Sb_x$ were presented. Sb doping has a strong impact on the CDW order and magnetic anisotropy of FeGe. Neutron diffraction investigations revealed that noncollinear magnetic structures develop in $FeGe_{1-x}Sb_x$ with a buckled kagome lattice which is substantially different from the magnetic structure in the parent compound, FeGe. We argue that this noncollinear antiferromagnetism might be unconventional and closely related to the kagome flat band. $FeGe_{1-x}Sb_x$ could become a new material platform to explore novel emergent phenomena related to kagome physics.

ACKNOWLEDGMENTS

We would like to thank Dr. A. Xu and Prof. S. Li from IOP for the support on additional magnetization measurements. This work was supported by the National Natural Science Foundation of China (Grants No. 12074426, No. 12004426, and No. 11227906), the Fundamental Research Funds for the Central Universities, the Research Funds of Renmin University of China (Grant No. 22XNKJ40), NSAF (Grant No. U2030106), and the Outstanding Innovative Talents Cultivation Funded Programs 2023 of Renmin University of China.

[1] J.-X. Yin, B. Lian, and M. Z. Hasan, Nature (London) **612**, 647 (2022).
[2] M. Kang *et al.*, Nat. Mater. **19**, 163 (2020).
[3] M. Li, Q. Wang, G. Wang, Z. Yuan, W. Song, R. Lou, Z. Liu, Y. Huang, Z. Liu, H. Lei, Z. Yin, and S. Wang, Nat. Commun. **12**, 3129 (2021).
[4] B. R. Ortiz, S. M. L. Teicher, Y. Hu, J. L. Zuo, P. M. Sarte, E. C. Schueller, A. M. M. Abeykoon, M. J. Krogstad, S. Rosenkranz, R. Osborn, R. Seshadri, L. Balents, J. He, and S. D. Wilson, Phys. Rev. Lett. **125**, 247002 (2020).
[5] K. Jiang, T. Wu, J.-X. Yin, Z. Wang, M. Z. Hasan, S. D. Wilson, X. Chen, and J. Hu, Natl. Sci. Rev. **10**, nwac199 (2023).
[6] F. Pollmann, P. Fulde, and K. Shtengel, Phys. Rev. Lett. **100**, 136404 (2008).
[7] Z. Lin, J.-H. Choi, Q. Zhang, W. Qin, S. Yi, P. Wang, L. Li, Y. Wang, H. Zhang, Z. Sun, L. Wei, S. Zhang, T. Guo, Q. Lu,

J.-H. Cho, C. Zeng, and Z. Zhang, Phys. Rev. Lett. **121**, 096401 (2018).

[8] B. C. Sales, J. Yan, W. R. Meier, A. D. Christianson, S. Okamoto, and M. A. McGuire, Phys. Rev. Mater. **3**, 114203 (2019).

[9] J.-X. Yin *et al.*, Nature (London) **583**, 533 (2020).

[10] S. Nakatsuji, N. Kiyohara, and T. Higo, Nature (London) **527**, 212 (2015).

[11] H. Li, T. T. Zhang, T. Yilmaz, Y. Y. Pai, C. E. Marvinney, A. Said, Q. W. Yin, C. S. Gong, Z. J. Tu, E. Vescovo, C. S. Nelson, R. G. Moore, S. Murakami, H. C. Lei, H. N. Lee, B. J. Lawrie, and H. Miao, Phys. Rev. X **11**, 031050 (2021).

[12] Y.-X. Jiang *et al.*, Nat. Mater. **20**, 1353 (2021).

[13] C. Mielke, III, D. Das, J.-X. Yin, H. Liu, R. Gupta, Y.-X. Jiang, M. Medarde, X. Wu, H. C. Lei, J. Chang, P. Dai, Q. Si, H. Miao, R. Thomale, T. Neupert, Y. Shi, R. Khasanov, M. Z. Hasan, H. Luetkens, and Z. Guguchia, Nature (London) **602**, 245 (2022).

[14] X. Feng, K. Jiang, Z. Wang, and J. Hu, Sci. Bull. **66**, 1384 (2021).

[15] M. M. Denner, R. Thomale, and T. Neupert, Phys. Rev. Lett. **127**, 217601 (2021).

[16] Y.-P. Lin and R. M. Nandkishore, Phys. Rev. B **104**, 045122 (2021).

[17] S.-Y. Yang, Y. Wang, B. R. Ortiz, D. Liu, J. Gayles, E. Derunova, R. Gonzalez-Hernandez, L. Šmejkal, Y. Chen, S. S. P. Parkin, S. D. Wilson, E. S. Toberer, T. McQueen, and M. N. Ali, Sci. Adv. **6**, eabb6003 (2020).

[18] F. H. Yu, T. Wu, Z. Y. Wang, B. Lei, W. Z. Zhuo, J. J. Ying, and X. H. Chen, Phys. Rev. B **104**, L041103 (2021).

[19] X. Teng *et al.*, Nature (London) **609**, 490 (2022).

[20] X. Teng, J. S. Oh, H. Tan, L. Chen, J. Huang, B. Gao, J.-X. Yin, J.-H. Chu, M. Hashimoto, D. Lu, C. Jozwiak, A. Bostwick, E. Rotenberg, G. E. Granroth, B. Yan, R. J. Birgeneau, P. Dai, and M. Yi, Nat. Phys. **19**, 814 (2023).

[21] J.-X. Yin *et al.*, Phys. Rev. Lett. **129**, 166401 (2022).

[22] Y.-P. Lin, C. Liu, and J. E. Moore, arXiv:2307.11810.

[23] H. Chen, Q. Niu, and A. H. MacDonald, Phys. Rev. Lett. **112**, 017205 (2014).

[24] Y. Zhang, Y. Sun, H. Yang, J. Železný, S. P. P. Parkin, C. Felser, and B. Yan, Phys. Rev. B **95**, 075128 (2017).

[25] A. K. Nayak, J. E. Fischer, Y. Sun, B. Yan, J. Karel, A. C. Komarek, C. Shekhar, N. Kumar, W. Schnelle, J. Kübler, C. Felser, and S. S. P. Parkin, Sci. Adv. **2**, e1501870 (2016).

[26] M. Kimata, H. Chen, K. Kondou, S. Sugimoto, P. K. Muduli, M. Ikhlas, Y. Omori, T. Tomita, A. H. MacDonald, S. Nakatsuji, and Y. Otani, Nature (London) **565**, 627 (2019).

[27] Y. Chen, J. Gaudet, S. Dasgupta, G. G. Marcus, J. Lin, T. Chen, T. Tomita, M. Ikhlas, Y. Zhao, W. C. Chen, M. B. Stone, O. Tchernyshyov, S. Nakatsuji, and C. Broholm, Phys. Rev. B **102**, 054403 (2020).

[28] B. B. Singh, K. Roy, J. A. Chelvane, and S. Bedanta, Phys. Rev. B **102**, 174444 (2020).

[29] See Supplemental Material at http://link.aps.org/supplemental/10.1103/PhysRevB.108.184431 for details on crystallographic data, susceptibility and transport data in polycrystalline samples, and neutron diffraction data at 4 K for $FeGe_{1-x}Sb_x$.

[30] P. Cheng, H. Zhang, W. Bao, A. Schneidewind, P. Link, A. Grünwald, R. Georgii, L. Hao, and Y. Liu, Nucl. Instrum. Methods Phys. Res., Sect. A **821**, 17 (2016).

[31] J. Rodríguez-Carvajal, Phys. B **192**, 55 (1993).

[32] X. Z. Yu, N. Kanazawa, Y. Onose, K. Kimoto, W. Z. Zhang, S. Ishiwata, Y. Matsui, and Y. Tokura, Nat. Mater. **10**, 106 (2011).

[33] A. M. Mills and A. Mar, J. Alloys Compd. **298**, 82 (2000).

[34] Q. D. Gibson, R. Daou, M. Zanella, J. Alaria, and M. J. Rosseinsky, Phys. Rev. B **108**, 035102 (2023).

[35] H. Yang *et al.*, Sci. Bull. **67**, 2176 (2022).

[36] G. Ding, H. Wo, Y. Gu, Y. Gu, and J. Zhao, Phys. Rev. B **106**, 235151 (2022).

[37] J. B. Forsyth, C. Wilkinson, and P. Gardner, J. Phys. F **8**, 2195 (1978).

[38] K. Yasukōchi, K. Kanematsu, and T. Ohoyama, J. Phys. Soc. Jpn. **16**, 429 (1961).

[39] J. Bernhard, B. Lebech, and O. Beckman, J. Phys. F **14**, 2379 (1984).